applied sciences

MDPI

Article

# The Preparation of Active Support-Based Sealing Material and Sealing Effect Analysis

**Jianguo Zhang [1,2], Yuejin Zhou [3,4,*], Xin Zhou [3,*], Man Wang [1,2], Shuaitao Liu [1,2], Zhanbiao Yang [1,2] and Lihui Zheng [3]**

1 State Key Laboratory of Coking Coal Resources Green Exploitation, Pingdingshan 467000, China; zhangjg_z@126.com (J.Z.); wangman_w@163.com (M.W.); cumt3136@163.com (S.L.); yzb0309@126.com (Z.Y.)
2 China Pingmei Shenma Holding Group Co., Ltd., Pingdingshan 467000, China
3 School of Mechanics and Civil Engineering, China University of Mining & Technology, Xuzhou 221116, China; lihuiz2021@163.com
4 State Key Laboratory for Geomechanics & Deep Underground Engineering, China University of Mining & Technology, Xuzhou 221116, China
* Correspondence: yuejinzh@163.com (Y.Z.); zhouxin3136@cumt.edu.cn (X.Z.); Tel.: +86-13914884696 (Y.Z.); +86-13880341506 (X.Z.)

**Abstract:** To improve the effect of gas drainage, with the aim of overcoming the problem of air leakage of conventional sealing materials, this study proposed the concept of gas drainage borehole sealing with active support and developed a new type of sealing material with the properties of permeability, fluidity, expansibility, early strength and compressive resistance through orthogonal tests. Using a specially designed active support testing device, this study analyzed the development law of borehole fracture under the action of active support force, which was then verified via field tests at a mine in Henan Province, China. The results show that the higher the expansion rate, the smaller the internal friction angle and cohesion, which is reflected in the sharp decline in the peak strength of the sealing material. The active support force of the sealing material has a significant time effect. It increases rapidly at first, before its growth rate slows down and tends toward a certain value. The greater the active support force provided by the sealing material, the smaller the radius of the plastic zone and breakage zone; this observation is also true of the displacement around the borehole. The active support force of sealed boreholes can effectively inhibit the development of cracks around the hole and reduce the generation of gas leakage channels. Under the action of the same burial depth and active support force, the larger the mechanical parameters of rock, the smaller the radius of the plastic zone and the breakage zone, as well as the smaller the displacement around the borehole. As has been proven by engineering practice, under the same conditions, the gas drainage concentration of the new sealing material is 47.5%, which is 84.8% higher than that of the original sealing material.

**Keywords:** active support; orthogonal test; fracture development; sealing effect; borehole sealing



**Citation:** Zhang, J.; Zhou, Y.; Zhou, X.; Wang, M.; Liu, S.; Yang, Z.; Zheng, L. The Preparation of Active Support-Based Sealing Material and Sealing Effect Analysis. *Appl. Sci.* **2023**, *13*, 8338. https://doi.org/10.3390/app13148338

Academic Editor: Syed Minhaj Saleem Kazmi

Received: 15 May 2023
Revised: 10 July 2023
Accepted: 13 July 2023
Published: 19 July 2023



## 1. Introduction

The mining of coal resources in deep mines is likely to face the predicament of “five highs and two disturbances”. In particular, the gas outburst caused by coal seams of high gas and low permeability seriously restricts the safe production and sustainable development of mines [1,2]. The fundamental way to effectively solve the problem of gas outburst is gas pre-pumping, and the key method that determines the effect of gas pre-pumping is the quality of sealing [3–7]. According to the statistics, the pre-pumping concentration of gas in about 65% of high-gas mines is lower than 30%, which can be attributed to the poor sealing quality of boreholes for gas drainage [8].

Currently, the commonly used sealing materials in China include polyurethane, cement-based material and high-water material [9–12]. As a polymer foaming material, polyurethane has the advantages of being lightweight, having a large expansion rate and being simple to operate. However, due to its poor permeability, it can not penetrate into the micro-fissures and fractures around the boreholes; due to its low strength and large compression deformation, it cannot provide support for the boreholes, thus causing poor borehole stability and gas leakage channels around the boreholes [13]. In addition, the foam rate of polyurethane is too high, frequently resulting in an insufficient sealing depth. In this case, the borehole and the roadway plastic zone would be connected to a gas leakage zone [14,15]. High-water material is widely used in goaf filling because of its simple filling process and low filling cost. In recent years, it has also been used in downhole sealing [16]. With the increase in the water–cement ratio, the grouting property and permeability of the high-water-content expansion material increased, while the strength and timeliness decreased [17]. However, the weathering characteristics of high-water materials lead to the weakening of the sealing effect with the extension of the extraction time [18]. Cement-based material is cheap and can be adjusted by adding additives; thus, it is widely used in borehole sealing. Scholars both at home and abroad have conducted a lot of research into the performance of cement-based sealing material [19–22]. As cement-based material is injected into the borehole, the surrounding rock is blocked and reinforced, thus greatly improving the gas-pumping effect [23,24]. However, the cement-based material can hardly provide active support for the borehole, which leads to its failure to reduce or inhibit the development of fractures during the initial sealing of the borehole. In the later stage of pumping, the cement-based material is prone to the phenomenon of water loss shrinkage, which reduces the gas-pumping effect [25]. The most common sealing materials used in mining are mainly made of expanded cement, although the traditionally used expanded cement has poor fluidity, low strength and certain shrinkage after setting, which creates slurry in the sealing material in the early stage of drilling and means that sealing cannot be fully injected into the cracks of coal and rock mass. Moreover, the shrinkage of the expanded cement after setting provides a new air leakage channel, which leads to only a small improvement in the stability of drilling. The gas leakage channel also reduces the efficiency of gas extraction [26].

In view of the shortages of different types of sealing materials, scholars have conducted a lot of research into the sealing materials used in extraction drilling in recent years. Kazuki [27] and Norachai [28] et al. studied the effect of the molecular structure of a high-efficiency water-reducing agent on the fluidity of a cement slurry sealing material, and the study showed that a smaller molecular structure was helpful in causing the dispersion of cement particles and improved the fluidity of the fluid slurry sealing material. When the polycarboxylic acid superplasticizer content is between 1.8 and 2.4%, the fluidity of the experimental cement is greatly increased. Gullu et al. [29] studied the effect of geopolymer sealing materials on the rheological properties of cement slurry. The rheological properties of cement slurry decreased with the increase in the water/binder ratio. Li et al. [30] studied the sealing performance of the sealing material used in pulverized coal drilling, and the research showed that the smaller the water/material ratio, the greater the expansion degree. According to the expansibility, strength and cost of the pulverized coal sealing material, the optimum composition ratio of the pulverized coal drilling sealing material was determined to be 70% fly ash and 30% dosage. At this time, the expansion rate and maximum compressive strength of the sealing material are 6% and 7.30 MPa, respectively. However, in the process of the development of sealing materials, no modification method has been found to improve the fluidity, strength and expansion of the sealing material at the same time. In the past, the development of sealing materials focused on improvements in a certain aspect of performance, and no sealing materials with high fluidity, high strength and expansion properties were developed. Therefore, in view of the problems existing in conventional sealing methods, this study started by studying the source of sealing gas leakage and proposed the concept of the active support sealing of gas drainage boreholes. On this basis, a new type of sealing material with permeability, fluidity, expansibility, early strength and compressive resistance was developed, which could provide active support for boreholes. Using this new material, crack development around the borehole could be inhibited, thus improving the efficiency of gas drainage in the later stage.

## 2. Sealing Material Preparation Based on Orthogonal Test

### 2.1. The Concept of Borehole Active Support Sealing

With the gas drainage borehole taken as a miniature circular roadway, the concept of borehole active support and sealing is proposed. Figure 1 is the schematic diagram of active support sealing. To be specific, with the help of grouting pressure, the primary active support force is applied to the borehole. The secondary active support force is applied to the borehole surrounding the rock depending on the expansibility of the sealing material in the later stage, so as to inhibit the development of cracks around the borehole. As the sealing material permeates into the cracks of the broken surrounding rock, the borehole can be sealed and reinforced accordingly.

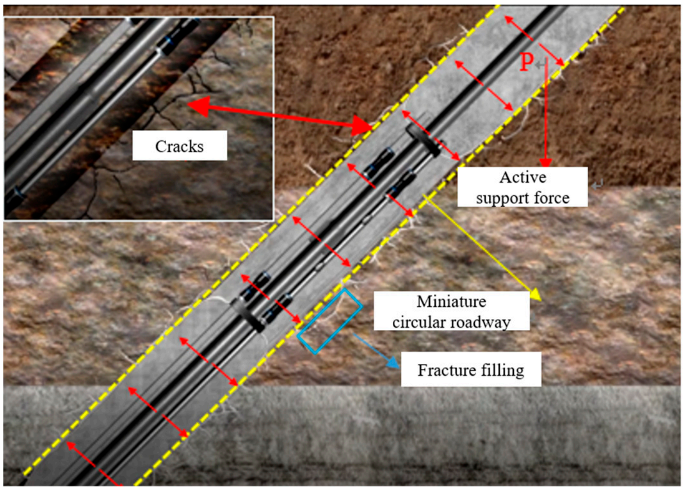


**Figure 1.** The schematic diagram of active support sealing.

### 2.2. Raw Materials and Test Method

#### 2.2.1. Selection of Raw Materials

To prepare a new sealing material with high expansibility, early strength and fluidity, Portland cement, quicklime, an accelerating agent, expanding agent, and fly ash are used to design the mix ratio of sealing materials, as is shown in Figure 2.

(1) Ordinary Portland Cement (OPC)

OPC of grade PO42.5 is used as the binder material for the sealing material.

(2) Lime

The CaO in lime reacts with the hydration product of cement, namely sulphoaluminate calcium, to produce ettringite. The more ettringite is produced, the higher the strength of the material. Additionally, the heat released during lime hydration accelerates the reaction of the material.

(3) Fly Ash

Fly ash mainly comes from the combustion of coal in thermal power plants. It has a small particle size, low density, and acts as a suspending agent that can reduce the water seepage rate of the sealing material. It also partially replaces some cement, reducing material costs.

(4) Expanding Agent

Cement-based materials tend to shrink due to water seepage, which can cause air-leakage channels to form between the sealing material and the borehole wall. Adding expanding agents to the material can compensate for the reduction in volume caused by water seepage, reducing the development of borehole fractures and providing additional support resistance. The expansion agent used in this experiment is a calcium sulfoaluminate expansion agent (CSA) produced by Wuhan Sanyuan Special Building Materials Co., LTD. (Wuhan, China), which is prepared by calcium sulfoaluminate (CAS), calcium aluminate (CA) and an appropriate amount of natural anhydrite and activator.

(5) Set Accelerator

The hydration reaction of cement is slower. Therefore, adding a set accelerator to the material can shorten the initial setting time. The set accelerator adopted is the PCS-3 rapid-setting and early-strength agent.

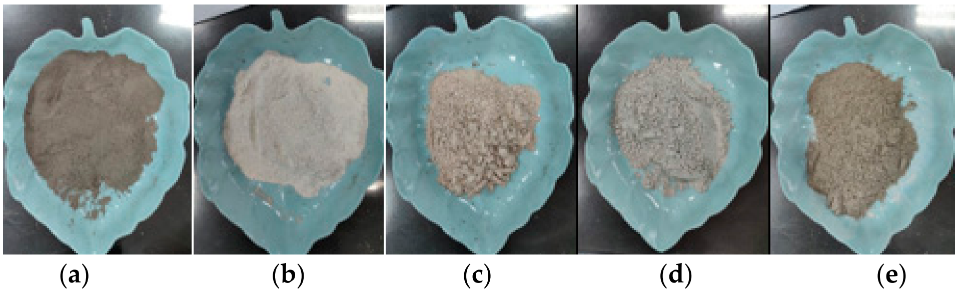


**Figure 2.** Raw materials for test: (**a**) Portland cement; (**b**) quicklime; (**c**) accelerating agent; (**d**) expanding agent; (**e**) fly ash.

#### 2.2.2. Test Method

The test contents include the material mobility, bleeding rate, initial setting time, expansion rate and compressive strength. The test scheme is shown in Figure 3.

(1) Fluidity

Before the test, prepare a smooth sheet with a side length of 50 cm, a truncated cone mold and a steel rule. Wipe the smooth sheet and the truncated cone mold with a wet rag, then pour the prepared slurry into a slightly wet truncated cone mold and smooth the slurry with a steel rule. After smoothing, quickly lift the truncated cone mold. The maximum diameter of the two directions perpendicular to each other of the slurry flow expansion is measured with a steel ruler, and the average value is taken as the fluidity of the slurry.

(2) Bleeding rate

For the bleeding rate of the material, refer to JC/T2153-2012 Test Method for Cement Bleeding Water. The test steps are as follows: weigh the mass $M_1$ of the measuring cylinder, pour the prepared slurry into the measuring cylinder, weigh the total mass $M_2$ of the measuring cylinder and the slurry, and then wait for 30 min for each interval.

The volume of bleeding is observed for 5 min until the bleeding disappears, and the water droplets are poured into a 25 mL measuring cylinder with a glue head dropper to read the mass $W_b$ of the water. The formula for calculating the bleeding rate of the material is as follows:

$$B_w = \frac{W_b}{(M_2 - M_1)\omega} \tag{1}$$

where $\omega$ denotes the moisture content of the slurry.

(3) Initial setting time

The test instrument used for the initial setting time of the material is a Vicar instrument. The test steps are as follows: place a small glass plate at the bottom of the test mold, record the time of initial mixing slurry, and then pour the prepared good slurry into the test mold. After a period of time, the test begins. When the scale number is observed to be about 4 mm, record this moment as the initial setting time of the material.

(4) Expansion rate

The test method used for the expansion rate of the sealing material is the standard JC/T 313-2009 Test Method for the expansion rate of expansion cement. The test mold is 25 mm × 25 mm × 280 mm, and the length change value of the test block is measured by the length ratio instrument.

(5) Compressive strength

The prepared test block was put into a standard curing box for 28 days. The size of the sample was a cube with a side length of 70.7 mm. The SNAS uniaxial testing machine was used to test the uniaxial compressive strength of the material.

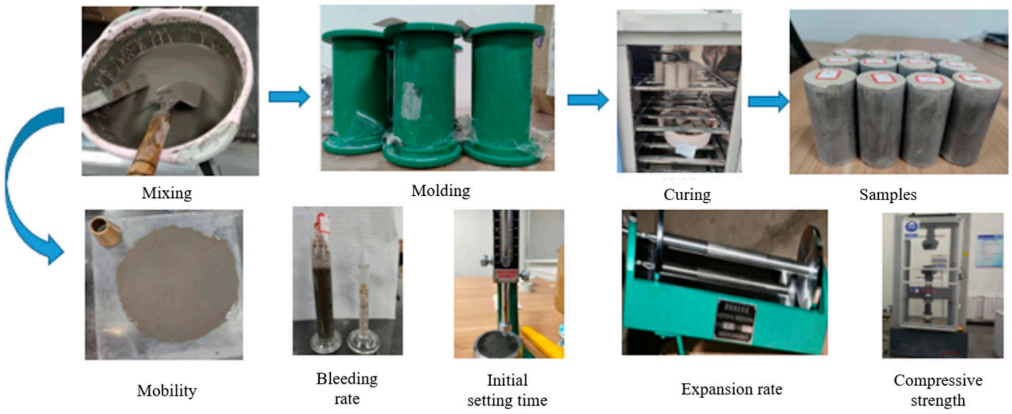


**Figure 3.** Test scheme.

### 2.3. The Design of Orthogonal Test

In the orthogonal test, the water/cement ratio, the content of quicklime, fly ash, accelerating agent, and expanding agent were set as influence factors. With the comprehensive consideration of the test scheme and actual needs, this study selected four levels of these five influence factors to conduct the orthogonal test. In total, 16 groups of tests were conducted. The influence factors and their respective levels are shown in Table 1. The content of each factor is denoted by their ratio with Portland cement.

**Table 1.** The factors and their levels in the test.

| Factors | the Water-Cement Ratio | the Content of Quicklime | Fly Ash | Accelerating Agent | Expanding Agent |
|---|---|---|---|---|---|
| level 1 | 0.9:1 | 0.12 | 0.20 | 0.05 | 0.05 |
| level 2 | 1:1 | 0.16 | 0.30 | 0.10 | 0.15 |
| level 3 | 1.1:1 | 0.20 | 0.40 | 0.15 | 0.25 |
| level 4 | 1.2:1 | 0.24 | 0.50 | 0.20 | 0.35 |

### 2.4. Analysis of Orthogonal Test Results

Table 2 shows the results of the sixteen groups of orthogonal tests. As can be seen, the fluidity of every water/cement ratio is greater than 250 mm. According to the relevant literature, the grouting material fluidity can meet the pumping requirements when it is greater than 140 mm [31]. Therefore, the fluidity of the materials is not considered in the comprehensive analysis of the orthogonal test. According to the comprehensive analysis based on the orthogonal test of the borehole sealing material in Figure 4a, the bleeding rate and initial setting time increase with the increase in the water/cement ratio; this is because, with the increase in the water/cement ratio, the water content in the material increases, which speeds up the water emission rate on the surface of the material, so the bleeding rate increases, and the relative contact area between the water and cement particles decreases; the reaction rate between the cement particles will slow down, and the initial setting time of the material will increase. In addition, the expansion rate and compressive strength decrease with the increase in the water–cement ratio; this is because the water/cement ratio increases and the porosity of the material increases, which leads to a reduction in the expansion rate and compressive strength of the concrete. For the borehole sealing grouting material, the smaller the bleeding rate is, the better. Ideally, the material is expected to set and solidify after the end of grouting. Generally, the time from adding the water and mixing material to the end of grouting is 20~40 min, so the water-cement ratio is 0.9:1. As can be seen from Figure 4b, with the increase in the quicklime content, the bleeding rate decreases first and then increases, and the expansion rate increases first and then slowly decreases. When the quicklime content is 0.2, the sealing material performs better in terms of the initial setting time, compressive strength, bleeding rate and expansion rate. Accordingly, the quicklime content is set to 0.2. As is shown in Figure 4c, the impact of the fly ash content on the compressive strength and expansion rate is small, and the initial setting time increases with the increase in the fly ash content. When the fly ash content is 0.3, the bleeding rate is relatively low and the initial setting time short. Therefore, the fly ash content is set to 0.3. From Figure 4d, it can be seen that the content of accelerating agent exerts a relatively weak influence on the compressive strength and expansion rate of the material; by contrast, its influence on the initial setting time and bleeding rate of the material is much stronger. With the increase in the accelerating agent content, the bleeding rate and initial setting time decrease significantly. When the accelerating agent content is greater than 0.15, the downward trend in the initial setting time is weakened. Accordingly, the content of the accelerating agent is set to 0.15. As can be seen from Figure 4e, the expanding agent exerts its greatest influence on the compressive strength and expansion rate. As the content of expanding agent increases, the compressive strength significantly decreases, whereas the expansion rate increases correspondingly. Therefore, the value near the intersection of the two curves of compressive strength and expansion rate should be selected for the expanding agent content. Accordingly, the expansion agent content is set to 0.2. To sum up, the contents of these raw materials are as follows: water-cement ratio: 0.9:1, quicklime: 0.2, fly ash: 0.3, accelerating agent: 0.15, and expanding agent: 0.2.

**Table 2.** The results of orthogonal tests.

| Groups | Bleeding Rate/% | Fluidity/mm | Initial Setting Time/h | Compressive Strength/MPa | Expansion Rate/% |
|---|---|---|---|---|---|
| 1 | 8.93 | 292 | 10.63 | 4.88 | 0.73 |
| 2 | 4.63 | 266 | 5.77 | 3.12 | 2.87 |
| 3 | 2.03 | 256 | 2.08 | 1.88 | 4.83 |
| 4 | 1.54 | 260 | 1.67 | 1.03 | 6.77 |
| 5 | 2.00 | 304 | 3.17 | 0.99 | 6.58 |
| 6 | 0.25 | 315 | 1.55 | 1.53 | 4.85 |
| 7 | 10.7 | 297 | 12.05 | 2.82 | 2.85 |
| 8 | 7.34 | 293 | 7.10 | 4.22 | 0.86 |
| 9 | 3.08 | 318 | 3.00 | 2.71 | 2.40 |
| 10 | 3.52 | 306 | 3.17 | 4.18 | 0.80 |
| 11 | 8.05 | 326 | 8.63 | 0.96 | 6.77 |
| 12 | 11.97 | 330 | 13.50 | 1.27 | 4.78 |
| 13 | 8.87 | 312 | 10.20 | 1.28 | 4.47 |
| 14 | 13.56 | 323 | 14.63 | 0.75 | 6.50 |
| 15 | 0.85 | 334 | 3.75 | 4.12 | 0.77 |
| 16 | 7.22 | 315 | 3.13 | 2.48 | 2.60 |

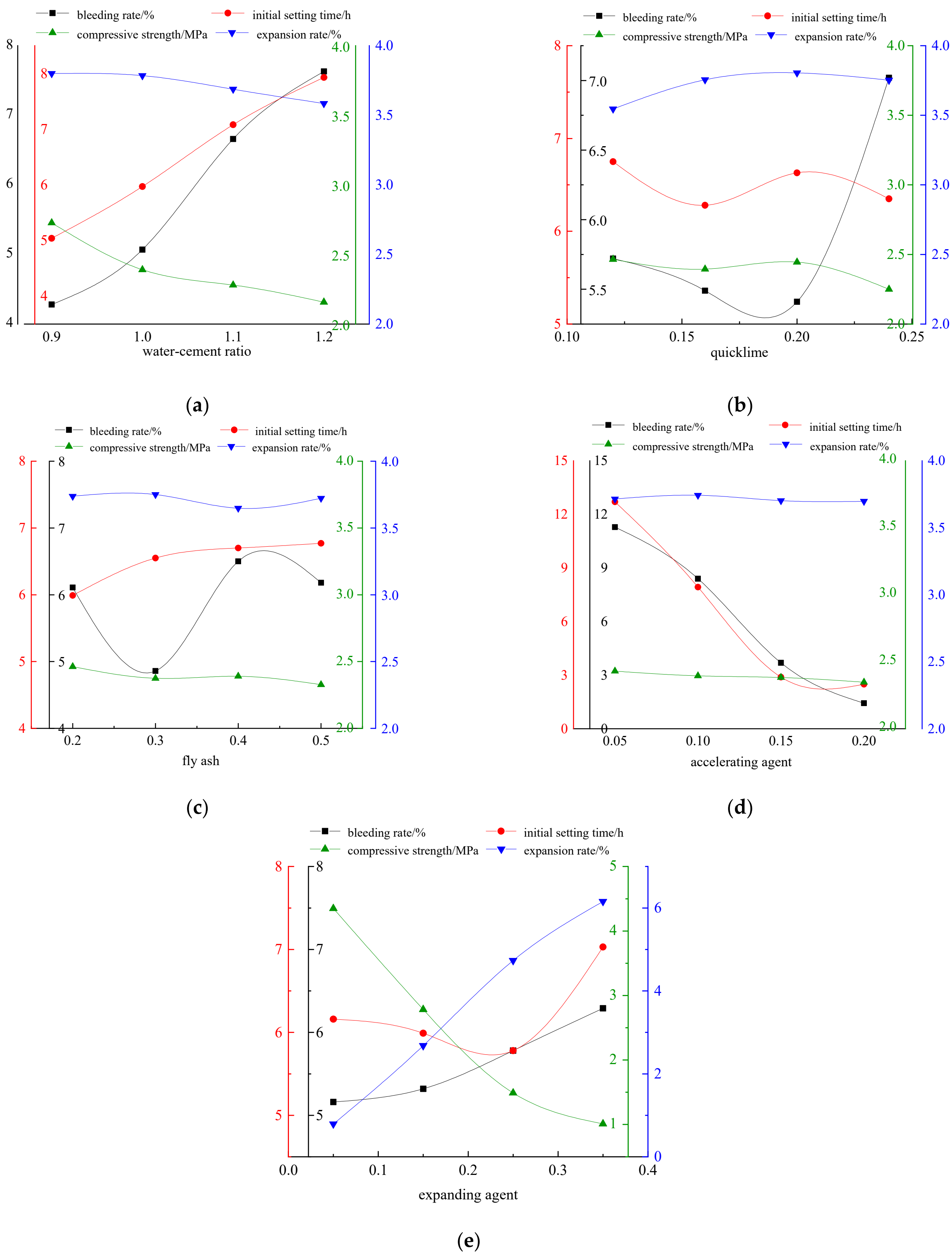


**Figure 4.** Comprehensive analysis diagram of orthogonal test of sealing material: (**a**) water/cement ratio; (**b**) quicklime content; (**c**) fly ash content; (**d**) accelerating agent content; (**e**) expanding agent content.

## 3. Analysis of Mechanical Characteristics of Sealing Material

### *3.1. TriAxial Strength and Deformation Characteristics*

Based on the ratio of the sealing materials obtained via orthogonal tests, the test specimens with different expansion rates, namely, 0%, 1%, 3% and 5%, were obtained by changing the content of expanding agent. The MTS815 electronic servo test system was used to conduct triaxial tests on the specimens, as shown in Figure 5. This test system mainly consists of oil sources, a testing machine, a confining pressure control cabinet, and a data acquisition system. The test specimens for the triaxial test were in a standard cylinder with a diameter of 50 mm and a height of 100 mm. The actual test scheme is as follows: Triaxial tests are carried out on the specimens with an expansion rate of 0%, 1%, 3% and 5%, respectively, and the loaded confining pressure grade gradients are 1 MPa, 2 MPa, and 3 MPa. Three tests are conducted for each group of specimens, with a total sample size of 36 specimens. The confining pressure is loaded at a rate of 0.01 MPa/s until it reaches the set value and then remains unchanged. Then the vertical load is applied via displacement control. In order to reflect the gradual and natural loading in the field, the loading rate was set at 0.01 mm/s until the specimen was damaged.

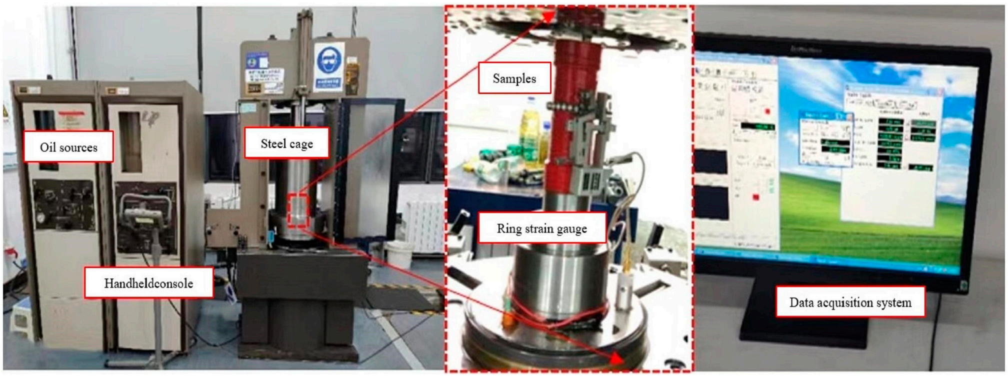


**Figure 5.** MTS815 electronic servo test system.

The triaxial test results for the sealing materials with different expansion rates are shown in Figure 6. As can be seen, the properties of the sealing materials change significantly with the size of the confining pressure. At a low confining pressure, the materials show the characteristics of brittle materials, and the stress decreases significantly with the increase in strain after specimen failure. When the confining pressure is relatively higher, the material shows the characteristics of a viscous material, and the post-peak stress is still more than 90% of the peak stress. With the increase in the confining pressure, the peak strength of the material also increases significantly. When the expansion rate is 1% and the confining pressure is 3 MPa, the peak strength is 10.14 MPa, and the corresponding peak strain increases as well. In general, the larger the lateral stress is, the more the curve of the elastic phase shifts to the left on the stress–strain curve. Accordingly, the greater the confining pressure is, the greater the elastic modulus of the material becomes and the stronger the deformation resistance of the material is. The annular strain of the specimen decreases with the increase in the confining pressure. Under the same confining pressure condition, the larger the expansion rate of the material is, the smaller the annular strain is. With the increase in the confining pressure, Poisson's ratio of the specimen decreases gradually. This is because the lateral pressure exerted on the specimen restricts its circumferential deformation to a certain extent under the higher confining pressure. The specimen's Poisson's ratio displays a downward trend with the increase in the expansion rate. This is because the larger the expansion rate of the specimen is, the more pores there are in the specimen, and the higher the compaction degree is under triaxial compression.

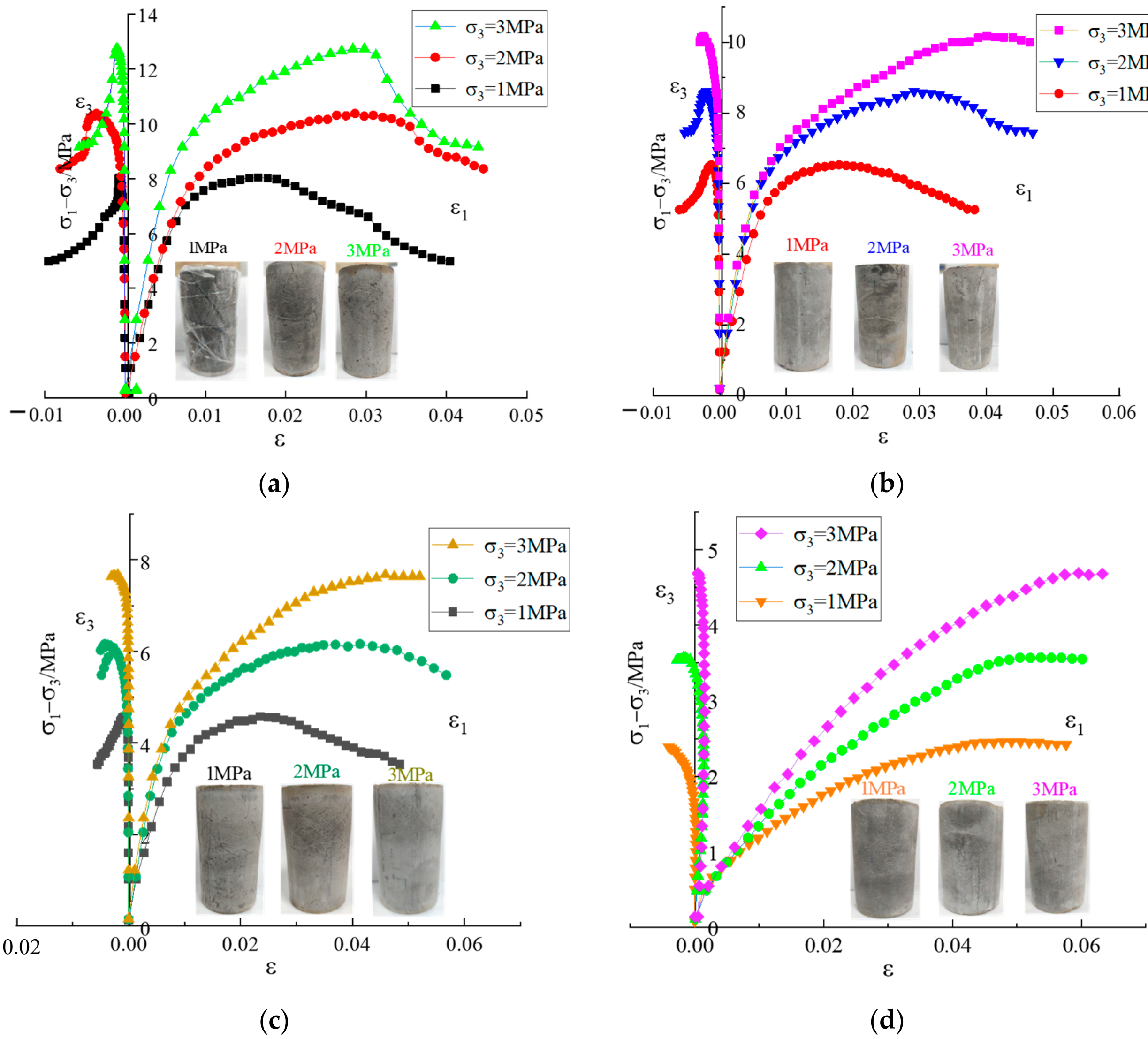


**Figure 6.** Triaxial compressive stress–strain curves for specimens with different expansion rates: (**a**) with an expansion rate of 0%; (**b**) with an expansion rate of 1%; (**c**) with an expansion rate of 3%; (**d**) with an expansion rate of 5%.

Figure 7 shows the curve of the elastic modulus of the sealing materials with different expansion rates when the confining pressure changes. As can be seen from the figure, the elastic modulus increases as the confining pressure rises; the higher the expansion rate is, the more the elastic modulus increases with the rise of the confining pressure. At a confining pressure of 3 MPa, the elastic modulus of the specimen with an expansion rate of 0% reaches 12.74 GPa, 38.6% higher than that of uniaxial compression. Similarly, at the same confining pressure, the elastic modulus of the specimen with an expansion rate of 5% reaches 1.53 GPa, 50% higher than that of uniaxial compression. By contrast, the increase in amplitude is greater than that of 0%. The larger the elastic modulus of the sealing material is, the greater its deformation resistance becomes, which is high.

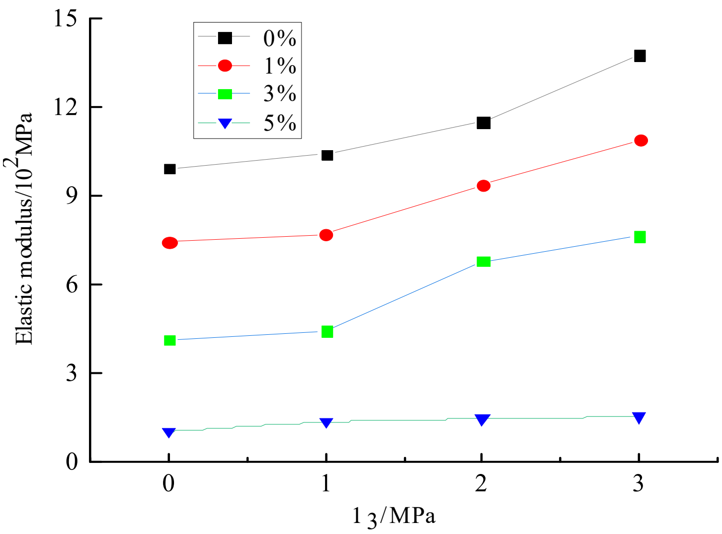


**Figure 7.** The relation curve of the confining pressure and elastic modulus.

According to the triaxial test data, the variation curve for the peak stress and confining pressure is shown in Figure 8. With the increase in the lateral stress, the peak stress of the specimen displays a linear growth trend. The lower the expansion rate of the sealing material is, the greater the slope of the variation curve of peak stress and confining pressure appears. In other words, with the increase in the confining pressure, the peak stress of the specimen with a lower expansion rate witnesses a sharper increase.

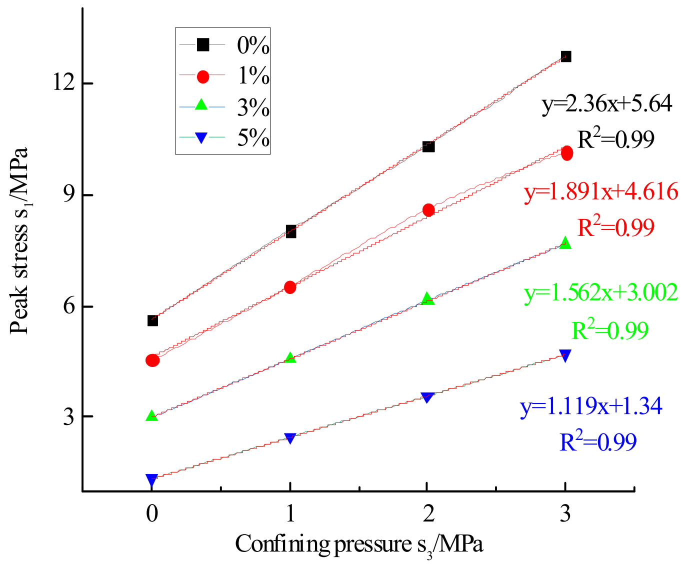


**Figure 8.** The relation curve of peak stress and confining pressure.

Based on the triaxial test data of the specimens at different confining pressures, the Mohr's circle strength envelope of stress was drawn to obtain its internal friction angle and cohesion, as shown in Table 3. With the increase in the expansion rate, the cohesion and internal friction angle of the specimens decrease accordingly. This is because the increase in the expansion rate leads to larger and more pores inside the specimen, which reduces the friction force and bite force between the particles of the specimen. The peak strength of the material decreases significantly due to the rapid decrease in the internal friction angle and cohesion. Different from the uniaxial failure mode, under the action of lateral stress, the triaxial failure mode is mainly shear failure.

**Table 3.** Internal friction angle and cohesion of specimens with different expansion rates.

| Expansion Rate | 0% | 1% | 3% | 5% |
|---|---|---|---|---|
| Cohesion C/MPa | 1.81 | 1.63 | 1.20 | 0.58 |
| Internal friction Angle φ/° | 25 | 23 | 16 | 10 |

### 3.2. Analysis of Active Support Force of Sealing Material

In order to study the active support force of sealing materials with different expansion rates, an active support force testing device is designed, which is mainly composed of an upper baseplate, lower baseplate, bolts and cylinder, as shown in Figure 9. The test mechanism of this device is as follows: The mixed grout is poured into a cylinder with an inner diameter of 50 mm. After a hydration reaction, volume expansion occurs in the grout, and the resulting expansive force is applied to the inner wall of the cylinder, resulting in the deformation of the inner wall. Four strain gauges are uniformly pasted around the cylinder wall to obtain the deformation. The expansive force of different sealing materials can be obtained by formula conversion, and the active support force calculation formula of sealing materials is [32] expressed as follows:

$$p = \frac{E\varepsilon\left[(r+\delta)^2 - r^2\right]}{2(1-\mu^2)r^2}, \tag{2}$$

where $p$ denotes the expansive force, MPa; $E$ represents the elastic modulus of the cylinder, MPa; $\mu$ is Poisson's ratio; $r$ denotes the inner diameter of the cylinder, mm; and $\delta$ refers to the thickness of the cylinder wall, mm.

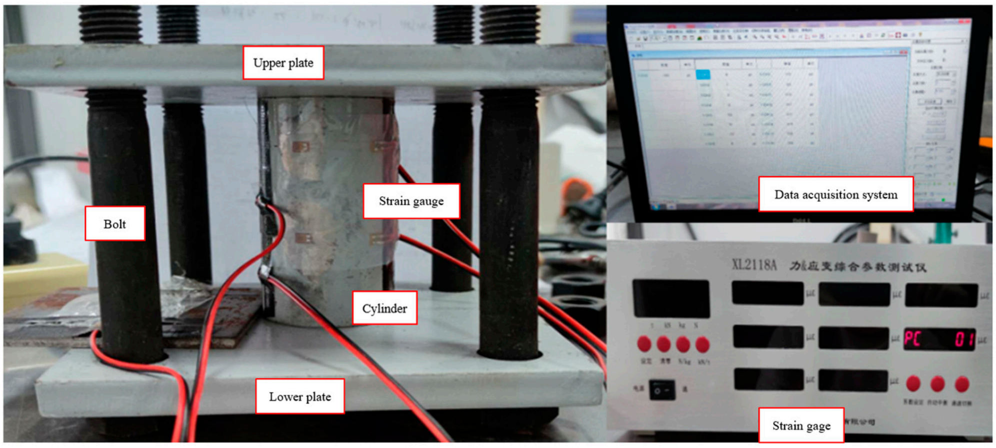


**Figure 9.** The active support force testing device.

Figure 10 shows the active support force–time curve of sealing materials with different expansion rates. As can be seen, the active support force of the sealing materials has a significant time effect. It increases rapidly at first, and then its growth rate slows down and tends toward a certain value. For the sealing materials with different expansion rates, the greater the expansion rate is, the greater active support force the material generates. When reacting for 24 h, the material with an expansion rate of 5% can provide an active support force of 1.44 MPa, and that of 3% and 1% can provide 0.68 MPa and 0.46 MPa, respectively. The maximum active support force that the material with an expansion rate of 5% can provide reaches 2.63 MPa, and that of 3% and 1% reaches 2.1 MPa and 1.4 MPa, respectively.

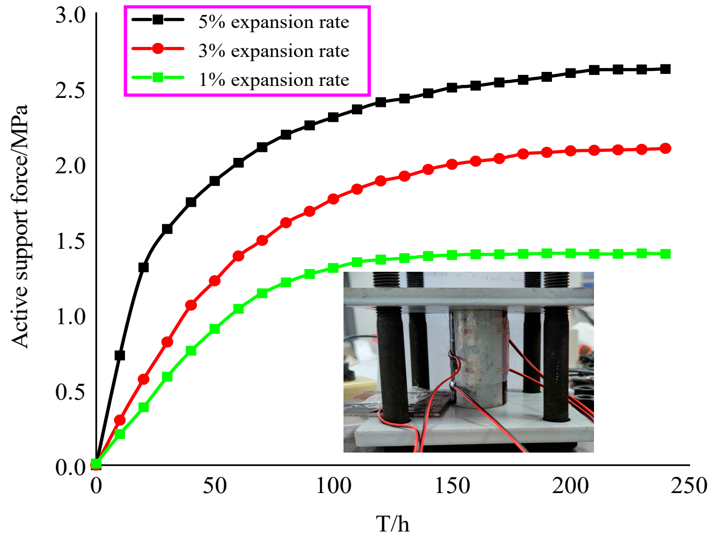


**Figure 10.** The active support force–time curve of sealing materials with different expansion rates.

## 4. Engineering Application

### *4.1. General Situation of the Working Face*

The 2404 belt bottom drainage roadway is located in the west wing of Shunhe Coal Mine. The layout area of the roadway is a monoclinic structure, and the strata are inclined to NW with a dip angle of 13~18°. Along the direction of tunneling, the apparent dip angle of the stratum is a 9~13° rise. The roadway is mainly located in the siltstone strata, 12 m below the No.2 coal floor, and its bedding relationship is shown in Figure 11. According to the drilling and sampling results in the west wing of Shunhe Coal Mine, the gas content of the No.2 coal seam in this area is 10.05 $m^3/t$, and the gas pressure is 0.56 MPa.

| Stratum | Thickness of stratum | Stratum section | Lithology |
|---|---|---|---|
| Coal(II) | 1.20~2.80 / 2.3 | | Black ~ steel gray, glass luster, block, mainly bright coal, semi-dark |
| Siltstone | 4.78~5.28 / 5.03 | | Gray to dark gray, top 0.3m mudstone, local sand less, bottom 0.81m fine sandstone. |
| Mudstone | 2.39~2.59 / 2.49 | | Dark gray ~ black, the upper part contains sandy, the lower contains plant fossil fragments and coal. |

**Figure 11.** Stratigraphic columns.

### *4.2. Theoretical Analysis of Borehole Areas under Active Support Force*

According to the concept that the gas drainage borehole is taken as a miniature round roadway, when the borehole is excavated, a broken ring plastic zone would be formed around the borehole. In other words, a fissure field is formed, as shown in Figure 12. The radius of the plastic zone around the borehole and that of the breakage zone can be calculated using Equations (2)–(4) [21].

$$R_p = R_0\left[\frac{(p_0 + c\cot\varphi)(1-\sin\varphi)}{(p_1 + c\cot\varphi)}\right]^{\frac{1-\sin\varphi}{2\sin\varphi}}, \tag{3}$$

$$R_s = R_0\left[\frac{(p_0 + c\cot\varphi)(1-\sin\varphi)}{(1+\sin\varphi)(p_1 + c\cot\varphi)}\right]^{\frac{1-\sin\varphi}{2\sin\varphi}}, \tag{4}$$

$$\mu = \frac{R_0 \sin\varphi}{2G} \frac{(p_0 + c\cot\varphi)^{\frac{1}{\sin\varphi}} (1 - \sin\varphi)^{\frac{1-\sin\varphi}{2\sin\varphi}}}{(p_1 + c\cot\varphi)^{\frac{1-\sin\varphi}{2\sin\varphi}}}, \tag{5}$$

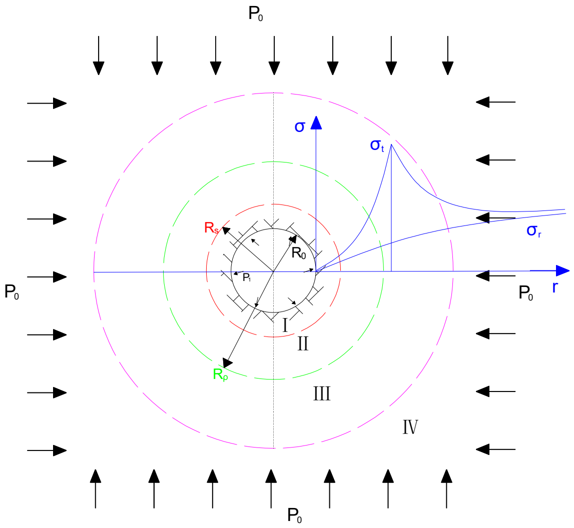


**Figure 12.** Stress distribution map of round borehole surrounding rock. I—breakage zone; II—plastic zone; III—elastic zone; IV—in situ stress zone.

The 2404 belt bottom drainage roadway adopts the method of drilling through strata. The borehole passes through mudstone and siltstone. Via the coring test of the borehole rock, its mechanical parameters are obtained and shown in Table 4. The burial depth of the 2404 belt bottom drainage roadway is 700 m, its ground stress is 17.5 MPa and the diameter of the borehole is 94 mm. The radius of the plastic zone of the borehole, that of the borehole breakage zone, and the displacement around the borehole can be calculated in two scenarios: with or without active support force. The calculation results are shown in Table 5.

**Table 4.** The mechanical parameters of mudstone and siltstone.

| Rock | Internal Friction Angle $\varphi$ | Cohesion c | Shear Modulus/MPa |
|---|---|---|---|
| mudstone | 30 | 1.20 | 347.2 |
| siltstone | 36 | 2.75 | 812.5 |

**Table 5.** The radius of the plastic zone and breakage zone, and the displacement around the borehole.

| Rock | Borehole Radius/mm | Active Support Force/MPa | Plastic Zone Radius/mm | Broken Zone Radius/mm | Surrounding Displacement/mm |
|---|---|---|---|---|---|
| mudstone | 99 | 2.63 | 135.5 | 99.7 | 16.9 |
| | | 2.10 | 143.9 | 104.2 | 17.9 |
| | | 1.40 | 157.7 | 111.2 | 19.6 |
| | | 0 | 204.0 | 130.8 | 25.5 |
| siltstone | 99 | 2.63 | 104.9 | 89.2 | 4.0 |
| | | 2.10 | 108.1 | 91.9 | 4.1 |
| | | 1.40 | 113.1 | 96.1 | 4.3 |
| | | 0 | 126.3 | 107.4 | 4.8 |

As can be determined from Table 5, with the increase in the active support force provided by the sealing material, the radius of the plastic zone and breakage zone decreases accordingly; the displacement around the borehole also displays a similar changing trend. This indicates that the active support force of the sealed borehole can effectively inhibit the development of cracks around the hole and reduce the generation of a gas leakage channel. At the same time, the mechanical properties of the borehole rock also have a great influence on the development of a borehole fissure. Under the action of the same burial depth and active support force, the larger the mechanical parameters of the rock are, the smaller the radius of the plastic zone and the breakage zone is, and the smaller the displacement around the borehole is.

### *4.3. The Project Examples of Borehole Areas under Active Support Force*

The borehole sealing test was conducted in the 2404 belt bottom drainage roadway of Shunhe Coal Mine. The bag-type borehole sealing device employed in this test was featured with “two plugging and two injections”; at the same time, the expansive cement-based material developed for this test was also used. In total, 28 boreholes were drilled, 24 of which were effective. Through the analysis of underground gas drainage data, it was found that the gas drainage concentration gradually decreases with the passage of the drainage time. Therefore, the drainage time with a high gas concentration and the negative pressure in the borehole were used to evaluate the sealing effect of the borehole. The 90-day gas drainage concentration and the negative pressure in the 24 boreholes were statistically analyzed, and then the analysis results were compared with the data for sealing with ordinary cement slurry. The results are shown in Figures 13 and 14, respectively.

Through the analysis and comparison of Figures 13 and 14, it can be determined that, with the application of the bag-type borehole sealing device, both the gas drainage concentration and negative pressure in the borehole are higher than those obtained with the original sealing technology. When the bag-type borehole sealing device is applied, the average drainage concentration during the first 15 days is 84.11%, displaying a relatively high stability and continuity; by contrast, the average drainage concentration when using the original sealing technology is 73.2%. When the drainage lasts for 90 days, the gas drainage concentration with the bag-type borehole sealing device is 47.5%, while that of the original sealing technology is only 25.7%. The gas drainage concentration is increased by 84.8%. It shows that the bag-type borehole sealing device featured with “two plugging and two injections” has a good sealing effect when using the newly developed expansive sealing material. Similarly, when the bag-type borehole sealing device is applied, the negative pressure is also higher than that when the original sealing technology is used. In addition, with the original sealing technology, the negative pressure decreases as the drainage time increases, indicating the existence of a gas leakage channel in the process of drainage.

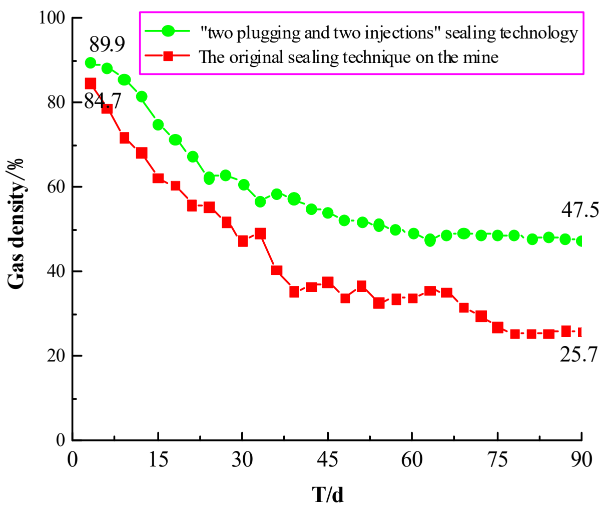


**Figure 13.** The comparison of gas drainage concentration.

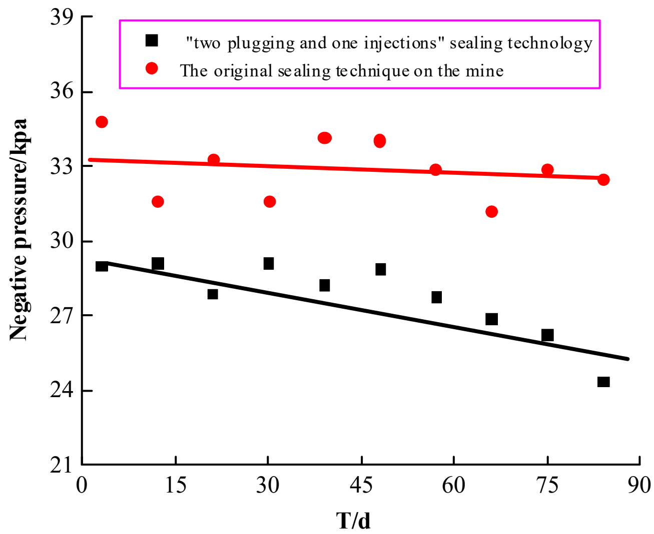


**Figure 14.** The comparison of negative pressure in the borehole.

## 5. Conclusions

(1) Based on the active support sealing concept of the gas drainage borehole, orthogonal tests were conducted to explore the mix ratio design of the sealing materials. On this basis, this study revealed the effects of the water/cement ratio, quicklime content, fly ash content, accelerating agent content and expanding agent content on the bleeding rate, fluidity, initial setting time, compressive strength and expansion rate of the sealing material. Through comprehensive analysis, the optimal combination of each factor is as follows: water/cement ratio: 0.9:1, quicklime content: 0.2, fly ash content: 0.3, accelerating agent content: 0.15, and expanding agent content: 0.2.

(2) The properties of the sealing materials vary significantly with the confining pressure. At a higher confining pressure, the material exhibits viscous material characteristics. Under the same confining pressure condition, the higher the expansion rate is, the smaller the annular strain is. The higher the expansion rate is, the smaller the internal friction angle and cohesion are, which is reflected by the sharp decline in the peak strength of the sealing material. The active support force of the sealing material has a significant time effect. It increases rapidly at first, and then its growth rate slows down and tends towards a certain value. The maximum active support force that the material with an expansion rate of 5% can provide reaches 2.63 MPa, and that of 3% and 1% reaches 2.1 MPa and 1.4 MPa, respectively.

(3) According to the active supporting force theory of sealing materials, with the increase in the active support force provided by the sealing material, the radius of the plastic zone and breakage zone decreases accordingly; the displacement around the borehole also displays a similar changing trend. This indicates that the active support force of the sealed borehole can effectively inhibit the development of cracks around the hole and reduce the generation of a gas leakage channel. At the same time, the mechanical properties of the borehole rock also have a great influence on the development of a borehole fissure. Under the action of the same burial depth and active support force, the larger the mechanical parameters of the rock are, the smaller the radius of the plastic zone and the breakage zone, and the smaller the displacement around the borehole.

(4) By analyzing the on-site gas drainage concentration and negative pressure, the bag-type borehole sealing technology featured with “two plugging and two injections” are more effective than the traditional sealing technology used in mining. When the drainage lasts for 90 days, the gas drainage concentration with the bag-type borehole sealing device is 47.5%, increasing by 84.8%. Similarly, when the bag-type borehole

sealing device is applied, the negative pressure is also higher than that using the traditional sealing technology.

**Author Contributions:** Conceptualization, J.Z., Y.Z. and X.Z.; methodology, J.Z.; software, J.Z.; validation, J.Z.; formal analysis, J.Z.; investigation, J.Z.; resources, J.Z.; data curation, J.Z.; writing—original draft preparation, J.Z.; writing—review and editing, Y.Z., X.Z., M.W., S.L., Z.Y. and L.Z.; visualization, J.Z.; supervision, J.Z.; project administration, J.Z.; funding acquisition, J.Z. All authors have read and agreed to the published version of the manuscript.

**Funding:** This research was funded by Open Research Fund of State Key Laboratory of Coking Coal Exploitation and Comprehensive Utilization, China Pingmei Shenma Group, grant NO. 41040220201132T, the National Key R&D Program of China, grant No. 2022YFE0129100, the National Natural Science Foundation of China, grant No.52061135111 and the China Postdoctoral Science Foundation, grant No. 2022M723396.

**Institutional Review Board Statement:** Not applicable.

**Informed Consent Statement:** Not applicable.

**Data Availability Statement:** The data presented in this study are available upon request from the corresponding author.

**Conflicts of Interest:** The authors declare no conflict of interest.

## References

1. Zhang, N.; Li, X.Y.; Zheng, X.G.; Xue, F. The status of deep coalmine and technical challenges. In Proceedings of the National Technology Conference of Kilometers Deep Coal Mine, Tai'an, China, 25 July 2013.
2. Zhang, N.; Chen, H.; Chen, Y. An engineering case of gob-side entry retaining in one kilometer-depth soft rock roadway with high ground pressure. *J. China Coal Soc.* **2015**, *40*, 494–501.
3. Zhou, F.B.; Xia, T.Q.; Wang, X.X.; Zhang, Y.F.; Sun, Y.N.; Liu, J.S. Recent Developments in Coal Mine Methane Extraction and Utilization in China: A Review. *J. Nat. Gas Sci. Eng.* **2016**, *31*, 437–458. [CrossRef]
4. Yuan, L. Strategic thinking of simultaneous exploitation of coal and gas in deep mining. *J. China Coal Soc.* **2016**, *41*, 1–6.
5. Zheng, K.G. Study on sealing technology of underground gas drainage boreholes of coal mines. *China Coal* **2017**, *43*, 109–114.
6. Lin, B.Q.; Lü, Y.C.; Li, B.Y.; Zhai, C. High-pressure abrasive hydraulic cutting seam technology and its application in outbursts prevention. *J. China Coal Soc.* **2007**, *32*, 959–963.
7. Lin, B.Q.; Wu, H.J.; Zhang, L.J.; Lu, H.L.; Zhang, H.B.; Meng, F.W. Integrative outburst prevention technique of high-pressure jet of abrasive drilling slotting. *Procedia Earth Planet. Sci.* **2009**, *1*, 27–34. [CrossRef]
8. Fu, J.H.; Cheng, Y.P. Situation of Coal and Gas Outburst in China and Control Countermeasures. *J. Min. Saf. Eng.* **2007**, *82*, 253–259.
9. Ge, Z.L.; Mei, X.D.; Lu, Y.Y.; Tang, J.R.; Xia, B.W. Optimization and Application of Sealing Material and Sealing Length for Hydraulic Fracturing Borehole in Underground Coal Mines. *Arab. J. Geosci.* **2015**, *8*, 3477–3490. [CrossRef]
10. Xue, C.; Zhang, L.L.; Wei, J.; Zhang, Y.; Xu, L.Z. Tests on impact resistance of modified cement-based sealing material for mine. *J. Saf. Sci. Technol.* **2020**, *16*, 70–75.
11. Zhang, H.T.; Li, Y.; Yao, B.H.; Wang, M. Time-dependent viscosity diffusion model of cement mortar grouting for gas drainage borehole sealing. *Coal Sci. Technol.* **2020**, *48*, 52–59.
12. Wang, H.; Wang, Q.P.; Min, F.F.; Chen, J. Research Progress of Grouting Sealing Materials. *Mater. Rep.* **2013**, *27*, 103–106.
13. Saleh, S.; Yunus, N.Z.M.; Ahmad, K.; Ali, N. Improving the Strength of Weak Soil Using Polyurethane Grouts: A Review. *Constr. Build. Mater.* **2019**, *202*, 738–752. [CrossRef]
14. Bian, X.; Ding, G.Q.; Wang, Z.F.; Cao, Y.P.; Ding, J.W. Compression and Strength Behavior of Cement-Lime-Polymer-Solidified Dredged Material at High Water Content. *Mar. Geores. Geotechnol.* **2017**, *35*, 840–846. [CrossRef]
15. Sun, Z.D. *Integrated Technology of Borehole Sealing and Fracture Blocking for Coal Seam Gas Extraction and the Application*; Henan Polytechnic University: Zhengzhou, China, 2021.
16. Xia, J.W.; Su, Q.; Liu, D.D. Optimal Gypsum-Lime Content of High Water Material. *Mater. Lett.* **2018**, *215*, 284–287. [CrossRef]
17. Hu, G.; He, W.; Lan, C. Sealing Behavior and Flow Mechanism of Expandable Material Slurry with High Water Content for Sealing Gas Drainage Boreholes. *Geofluids* **2018**, *2018*, 2954306. [CrossRef]
18. Wang, N.; Wang, Z.M.; Sun, Y.N.; Sun, Z.D.; Ding, L.P.; Fu, M.H. Optimization on PC-CAS based borehole sealing material for gas extraction and analysis of its expansion effect. *J. Saf. Sci. Technol.* **2020**, *16*, 77–82.
19. Zhang, T.J.; Bao, R.Y.; Li, S.G.; Zhang, C.; Zhang, L.; Jiang, X.K. Experimental study on expansion and creep characteristics of new CF sealing material. *J. Min. Saf. Eng.* **2019**, *36*, 175–183.
20. Wang, Z.F.; Zhou, Y.; Sun, Y.N.; Wang, Y.L. Novel gas extraction borehole grouting sealing method and sealing mechanism. *J. China Coal Soc.* **2015**, *40*, 588–595.

21. Zhang, C.; Chang, J.; Li, S.G.; Liu, C.; Qin, L.; Bao, R.Y.; Liu, H.; Cheng, R.H. Experimental Study Comparing the Microscopic Properties of a New Borehole Sealing Material with Ordinary Cement Grout. *Environ. Earth Sci.* **2019**, *78*, 149.
22. Zhang, C.; Liu, H.; Li, S.G.; Liu, C.; Qin, L.; Chang, J.; Cheng, R.H. Experimental Study on the Expansion of a New Cement-Based Borehole Sealing Material Using Different Additives and Varied Water–Cement Ratios. *Arab. J. Sci. Eng.* **2019**, *44*, 8717–8725. [CrossRef]
23. Wang, Z.M.; Sun, Y.N.; Song, W.B.; Wang, Y.L. Study on expansion mechanism and application of double-expansive material for borehole sealing in gas drainage. *J. Saf. Sci. Technol.* **2018**, *14*, 28–33.
24. Wang, Z.M.; Sun, Y.N.; Wang, Y.L.; Zhang, J.X.; Sun, Z.D. A Coupled Model of Air Leakage in Gas Drainage and an Active Support Sealing Method for Improving Drainage Performance. *Fuel* **2019**, *237*, 1217–1227. [CrossRef]
25. Liu, J.; Tang, T.T.; Lu, T.; Ji, X.L.; Qian, L. Activation effect of the fly ash with nano silicon nitride on the early strength properties of the mining-left cement sealing materials. *J. Saf. Environ.* **2020**, *20*, 1752–1757.
26. Zhang, T.; Bao, R.; Li, S. Expansion properties and creep tests for a new type of solidified expansive sealing material for gas drainage boreholes in underground mines. *Environ. Earth Sci.* **2018**, *77*, 468. [CrossRef]
27. Kazuki, M.; Daiki, S.; Hirokatsu, K. Effect of non-adsorbed superplasticizer molecules on fluidity of cement paste at low water-powder ratio. *Cem. Concr. Compos.* **2019**, *97*, 218–225.
28. Wongkornchaowalit, N.; Lertchirakarn, V. Setting Time and Flowability of Accelerated Portland Cement Mixed with Polycarboxylate Superplasticizer. *J. Endod.* **2011**, *37*, 387–389. [CrossRef]
29. Güllü, H.; Cevik, A.; Al-Ezzi, K.M.; Gülsan, M.E. On the rheology of using geopolymer for grouting: A comparative study with cement-based grout included fly ash and cold bonded fly ash. *Constr. Build. Mater.* **2019**, *196*, 594–610. [CrossRef]
30. Li, H.; Guo, S.S.; Chen, H.D. Application of coal-powder borehole-sealing material in borehole-sealing engineering. *Emerg. Mater. Res.* **2019**, *8*, 290–296. [CrossRef]
31. Gao, X.L. Elasto-Plastic Analysis of an Internally Pressurized Thick-Walled Cylinder Using a Strain Gradient Plasticity Theory. *Int. J. Solids Struct.* **2003**, *40*, 6445–6455. [CrossRef]
32. Jing, H.W.; Meng, Q.B.; Zhu, J.F.; Meng, B.; Yu, L.Y. Theoretical and technical progress of stability control of broken rock zone of deep roadway surrounding rock. *J. Min. Saf. Eng.* **2020**, *37*, 429–442.